

## Dynamical structure factor of an electron liquid. II

K. Awa

*Department of Physics, Hokkaido University, Sapporo 060, Japan*

H. Yasuhara

*College of Arts and Sciences, Tohoku University, Sendai 980, Japan*

T. Asahi

*Department of Physics, Hokkaido University, Sapporo 060, Japan*

(Received 6 July 1981; revised manuscript received 30 November 1981)

The dynamical structure factor  $S(q, \omega)$  of an electron liquid at metallic densities is studied numerically on the basis of the quasi-one-pair excitation approximation obtained in the preceding paper. The spin-averaged local field correction  $G(q)$  is estimated numerically; the local field correction  $C(q)$  arising from only spin-antiparallel correlation is also estimated. It is pointed out that inclusion of short-range correlations is important for the quantitative estimation of the energy width of the quasiparticle  $\Gamma(p)$  at metallic densities. Owing to the local field corrections and the energy width of the quasiparticle, the cutoff wave number  $q_c$  estimated by the present theory is considerably reduced, compared with the random-phase approximation case. The spectral structure in  $S(q, \omega)$  is numerically estimated from the wave number much smaller than  $q_c$  up to the wave number twice as large as the Fermi wave number. The calculated plasmon dispersion around  $q_c$  is in excellent agreement with the observed one for Al in electron scattering experiments. In the intermediate wave-number region the calculated spectra of  $S(q, \omega)$  reproduce distinctly a plasmonlike peak and a broad peak in good agreement with experimental observations. These characteristic features of  $S(q, \omega)$  are ascribed to the striking damping effect of one-electron states originating from virtual plasmon emission under the influence of strong short-range correlations at metallic densities.

## I. INTRODUCTION

The characteristic features of the dynamical structure factor  $S(q, \omega)$  of an electron liquid in the long-wavelength region can, in principle, be understood by means of the RPA.<sup>1,2</sup> There appear the well-defined plasmon excitation and the individual excitations. The quantitative description of  $S(q, \omega)$  in the random-phase approximation (RPA), however, becomes less adequate as the wave number  $q$  approaches the vicinity of the cutoff wave number  $q_c$ .<sup>3-7</sup> The plasmon peak there has a considerable amount of width. Its dispersion is lowered, compared with the RPA case. For the intermediate wave numbers beyond  $q_c$  the RPA description of  $S(q, \omega)$  at metallic densities is no longer adequate, even qualitatively.<sup>7,8</sup> In the preceding paper we have obtained the expression for  $S(q, \omega)$  in the quasi-one-pair excitation approximation which is adequate even for the intermediate wave-number

region. The purpose of this paper is to study numerically the spectral structure in  $S(q, \omega)$  from very small wave numbers up to the wave number twice as large as the Fermi wave number  $p_F$ , based on the quasi-one-pair excitation approximation.<sup>9</sup>

Electron correlations at metallic densities may be characterized by strong short-range correlations and the existence of higher-order excitations such as two-pair excitations and one-pair-plasmon excitations. In the framework of the quasi-one-pair excitation approximation these effects are represented by two quantities, the local field correction  $G(q)$  and the energy width of the quasiparticle  $\Gamma(p)$ . The local field correction  $G(q)$  important in the intermediate wave-number region is reasonably evaluated by inclusion of the particle-particle ladder vertex. The quantitative evaluation of the energy width  $\Gamma(p)$  at metallic densities may be achieved by including systematically local field corrections to the RPA expression for  $\Gamma(p)$ . The

two quantities  $G(q)$  and  $\Gamma(p)$  evaluated in a consistent manner not only make the plasmon dispersion much more flattened around  $q_c$  than that in the RPA but also reduce  $q_c$  itself by a considerable amount, as has been suggested<sup>10</sup> by DuBois at an early stage. The continuation of the plasmonlike peak into the one-pair continuum as well as the broad peak can also be reproduced in good agreement with experimental observations.

In Sec. II the numerical estimation of  $G(q)$  and  $\Gamma(p)$  will be given. In Sec. III the spectral shape of  $S(q, \omega)$  for wave numbers smaller than  $p_F$  will be discussed quantitatively. In Sec. IV the spectral structure in the intermediate wave-number region will be discussed in comparison with the observed spectra in x-ray<sup>7,8</sup> and electron<sup>3-6</sup> scattering experiments. The last section will be devoted to concluding remarks.

## II. LOCAL FIELD CORRECTION AND ENERGY WIDTH

In this section we shall study numerically  $G(q)$  and  $\Gamma(p)$  after making a compact statement of the

quasi-one-pair excitation approximation obtained in the preceding paper.<sup>9</sup> The dynamical structure factor  $S(q, \omega)$  for  $\omega \geq 0$  is related to the imaginary part of the inverse dielectric function. The dielectric function  $\epsilon(q, \omega)$  is written in terms of the proper polarization function  $\pi(q, \omega)$ :

$$S(q, \omega) = -[\pi v(q)]^{-1} \text{Im}[1/\epsilon(q, \omega)], \quad (1)$$

$$\epsilon(q, \omega) = 1 + v(q)\pi(q, \omega), \quad (2)$$

where  $v(q)$  is the Coulomb interaction. In the quasi-one-pair excitation approximation  $\pi(q, \omega)$  can be written as

$$\pi(q, \omega) = \frac{\tilde{\pi}^{(0)}(q, \omega)}{1 - G(q)v(q)\tilde{\pi}^{(0)}(q, \omega)}. \quad (3)$$

Here,  $\tilde{\pi}^{(0)}(q, \omega)$  is the free polarization function with energy widths of one-electron states included:

$$\tilde{\pi}^{(0)}(q, \omega) = -2 \int \frac{d\vec{p}}{(2\pi)^3} \left[ \frac{f(p)[1-f(\vec{p}+\vec{q})]}{\omega + i[\Gamma(p) - \Gamma(\vec{p}+\vec{q})] + \epsilon_p - \epsilon_{\vec{p}+\vec{q}}} - \frac{f(\vec{p}+\vec{q})[1-f(p)]}{\omega + i[\Gamma(\vec{p}+\vec{q}) - \Gamma(p)] + \epsilon_p - \epsilon_{\vec{p}+\vec{q}}} \right], \quad (4)$$

where  $f(p)$  denotes the Fermi distribution function at zero temperature and  $\epsilon_p$  is the free-electron energy. The local field correction  $G(q)$  and the energy width of the quasiparticle or the quasihole  $\Gamma(p)$  are given as follows:

$$-G(q)v(q) = \frac{1}{2} \langle I(\vec{p}, \vec{p}'; \vec{q}) - v(q) \rangle_{\vec{p}, \vec{p}'} + \frac{1}{2} \langle I(\vec{p}, \vec{p}'; \vec{q}) - v(q) - I(\vec{p}, \vec{p}'; \vec{p} - \vec{p}' + \vec{q}) \rangle_{\vec{p}, \vec{p}'}, \quad (5)$$

$$\Gamma(p) = \int \frac{d\vec{q}}{(2\pi)^3} v(q) [1 - G(q)] [1 - C(q)] \text{Im} \left[ \frac{1}{\epsilon(q, \epsilon_p - \epsilon_{\vec{p} - \vec{q}})} \right] \times [\Theta(\epsilon_p - \epsilon_{\vec{p} - \vec{q}}) - \Theta(\epsilon_F - \epsilon_{\vec{p} - \vec{q}})], \quad \Theta(x) = \begin{cases} 1, & x > 0 \\ 0, & \text{otherwise} \end{cases}. \quad (6)$$

Here,  $\epsilon_F$  is the Fermi energy and  $I(\vec{p}, \vec{p}'; \vec{q})$  the particle-particle ladder vertex<sup>12</sup> which is the solution of the integral equation

$$I(\vec{p}, \vec{p}'; \vec{q}) = v(q) + \int \frac{d\vec{k}}{(2\pi)^3} v(\vec{q} - \vec{k}) \frac{[1 - f(\vec{p} + \vec{k})][1 - f(\vec{p}' - \vec{k})]}{\epsilon_p - \epsilon_{\vec{p} + \vec{k}} + \epsilon_{\vec{p}' - \vec{k}}} I(\vec{p}, \vec{p}'; \vec{k}). \quad (7)$$

The angular bracket  $\langle \rangle_{\vec{p}, \vec{p}'}$  denotes an averaged value over  $\vec{p}$  and  $\vec{p}'$  within Fermi spheres. For the dielectric function entering in  $\Gamma(p)$  of Eq. (6) we employ the Hubbard type<sup>11</sup> of dielectric function with the local field correction  $G(q)$  of Eq. (5):

$$\epsilon(q, \omega) = 1 + v(q) \frac{\pi^{(0)}(q, \omega)}{1 - G(q)v(q)\pi^{(0)}(q, \omega)}, \quad (8)$$

where  $\pi^{(0)}(q, \omega)$  is the free polarization function. Note that a different type of local field correction

$C(q)$  in addition to  $G(q)$  enters in Eq. (6). This is the local field correction arising from spin-antiparallel correlation alone and is defined as

$$-C(q)v(q) = \langle I(\vec{p}, \vec{p}'; \vec{q}) - v(q) \rangle_{\vec{p}, \vec{p}'}. \quad (9)$$

We shall estimate numerically  $G(q)$ ,  $C(q)$ , and  $\Gamma(P)$  and mention their behaviors as a function of the wave number and the electron density.

#### A. $G(q)$ and $C(q)$

Let us first mention the local field correction arising from spin-parallel correlation which is given by the second term on the right-hand side of Eq. (5). We may there neglect higher-order terms with respect to the Coulomb interaction, since two electrons with parallel spins are originally forbidden to be close to each other owing to the Pauli principle. It can obviously be seen that for large momentum transfers higher-order direct terms are almost canceled by the corresponding exchange terms. In other words, a shape of the so-called Fermi hole is not expected to be appreciably affected by inclusion of the Coulomb interaction. Therefore we may estimate that correction in lowest-order approximation. An averaged value of  $v(\vec{p} - \vec{p}' + \vec{q})$  is chosen to be  $4\pi e^2/(q^2 + p_F^2)$ , as Hubbard first did.<sup>11</sup> So far as one is concerned with the spin-parallel correlation, Hubbard's local field correction is fairly good.

On the other hand, the local field correction arising from spin-antiparallel correlation is strongly affected by inclusion of the Coulomb interaction. An averaging of  $I(\vec{p}, \vec{p}'; \vec{q})$  over  $\vec{p}$  and  $\vec{p}'$  within Fermi spheres may be represented approximately by its value at  $\vec{p} = \vec{p}' = 0$ . An approximate solution for  $I(0, 0; q)$  obtained by one of us<sup>12</sup> (H. Y.) is written as

$$\begin{aligned} \langle I(\vec{p}, \vec{p}'; \vec{q}) \rangle_{\vec{p}, \vec{p}'} &\simeq v(q)A(\lambda)F(q, \lambda), \\ F(q, \lambda) &= 2 \left[ \frac{2}{2^{3/2}(2\lambda p_F/q)^{1/2}} \right]^2 \\ &\quad \times I_2[2^{3/2}(2\lambda p_F/q)], \\ A(\lambda) &= 2\lambda^{1/2}/I_1(4\lambda^{1/2}), \\ \lambda &= \alpha r_s/\pi, \quad \alpha = \left[ \frac{4}{9\pi} \right]^{1/3} = 0.52106\dots, \end{aligned} \quad (10)$$

where  $I_1(x)$  and  $I_2(x)$  are the first- and second-order modified Bessel functions, respectively, and  $r_s$  is the usual density parameter. The local field correction  $G(q)$  which is an average of spin-parallel and spin-antiparallel correlations is calculated with Hubbard's local field correction and Eq. (10) for  $q \geq p_F$  where  $G(q)$  plays an essential role. On the other hand, for  $q \leq p_F$  Eq. (5) is rather inappropriate. For such a wave-number region we then make an extrapolation in a form of

$G(q) = \alpha q^2 + \beta q^3 + \gamma q^4$  so as to reproduce the value at  $q = p_F$  and its derivative. The coefficient  $\alpha$  is chosen to reproduce the value of the compressibility in the Hartree-Fock approximation, which is fairly good even at metallic densities. The other coefficients  $\beta$  and  $\gamma$  are determined by the extrapolation procedure.

Another local field correction  $C(q)$  arising from spin-antiparallel correlation alone is calculated in a similar manner. For  $q \leq p_F$  an extrapolation in a form of  $C(q) = \beta' q^3 + \gamma' q^4$  is made so as to reproduce the value at  $q = p_F$  and its derivative; we omit a term of order  $q^2$  there, considering that spin-antiparallel correlation makes a minor contribution to the compressibility.

Calculated values of  $G(q)$  by the present theory together with those by other authors<sup>11,13,14</sup> are shown in Fig. 1 for  $r_s = 2.0$ . The present value of  $G(q)$  increases monotonously as a function of  $q$ . Let us first compare it with Hubbard's  $G(q)$ . It can be seen that the contribution from spin-antiparallel correlation plays an important role; the difference between the two comes from this correlation. Next we compare our local field correction  $G(q)$  with those by Vashishta and Singwi, and Lowy and Brown. Values of our  $G(q)$  are smaller than Lowy-Brown's values for any  $q$ , and are also smaller than the Vashishta-Singwi values for  $q \gtrsim 1.6p_F$ . The following fact should, however, be noted here. The two forms for the local field correction have been proposed primarily aiming at an adequate description of the pair distribution function  $g(r)$  at short distances. On the other hand, our form for  $G(q)$  is defined properly for the purpose of describing dynamical aspects of electron correlations and is founded on fundamental consideration. As has been elucidated in the preceding paper, not all higher-order corrections to the RPA that are required for the fulfillment of  $g(r) \geq 0$  for all densities can be reduced in a natural way into a form of the local field correction  $G(q)$ . In this sense one must be careful in comparing our form for  $G(q)$  with other authors' forms.

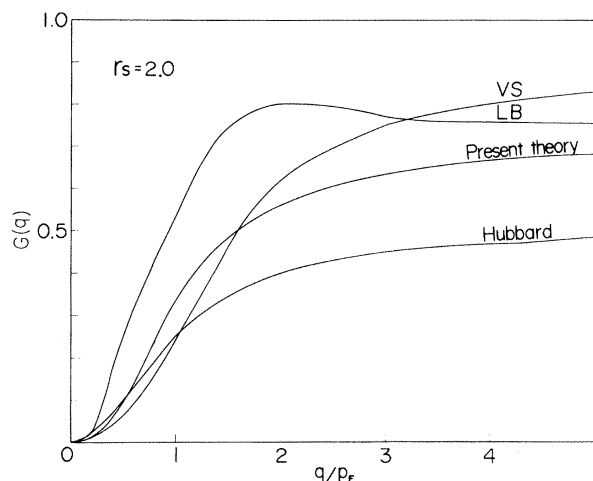


FIG. 1. A comparison of various forms of the local field correction  $G(q)$  for  $r_s = 2.0$ . VS: Vashishta-Singwi (Ref. 13). LB: Lowy-Brown (Ref. 14). Hubbard: J. Hubbard (Ref. 11). Present theory: Eq. (5).

We shall here make a comment about a singularity of  $G(q)$  reported in the literature.<sup>15,16</sup> Several authors have found that the local field correction exhibits a logarithmic singularity at  $q = 2p_F$  and

that it has a peak at a certain value of  $q$  somewhat smaller than  $2p_F$ . As is well known,<sup>17</sup> the self-energy correction in the Hartree-Fock approximation

$$\Sigma_{\text{HF}}(p) = \int d\vec{p}' / (2\pi)^3 v(\vec{p} - \vec{p}') f(p')$$

exhibits a similar singularity at  $p = p_F$ , which originates from long-wavelength components of the bare Coulomb interaction and the sharpness of the Fermi distribution function. It is, however, spurious and can be removed by the screening effect. The above singularity of  $G(q)$  at  $q = 2p_F$  can also be traced back to the same origin and probably is not intrinsic.

In Fig. 2, calculated values of  $G(q)$  are shown for various electron densities. It can be seen that the magnitude of  $G(q)$  for any value of  $q$  increases monotonously as  $r_s$  increases. It implies that the local field correction is still more important as the electron density is lowered. It is noted here that  $G(q)$  of our choice for  $q \geq p_F$  tends to 1, as  $r_s$  becomes exceedingly large. In the high-density limit, on the other hand, it is reduced to that of Hubbard. In Fig. 3 calculated values of  $C(q)$  are also shown for various electron densities.

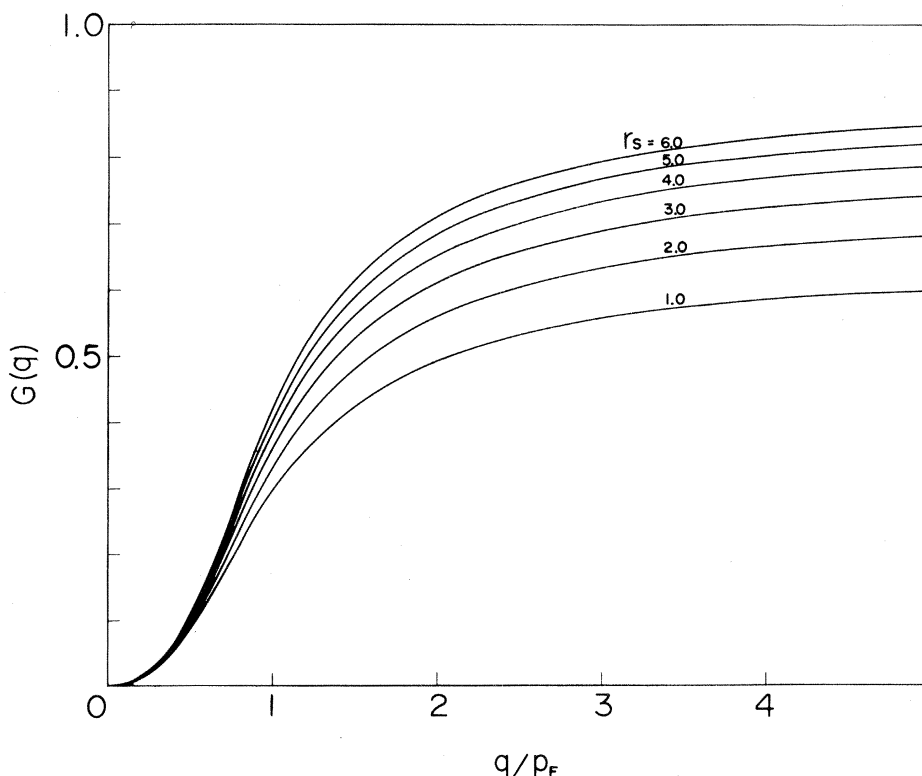


FIG. 2. Calculations of the local field correction  $G(q)$  in the present theory for various values of  $r_s$ .

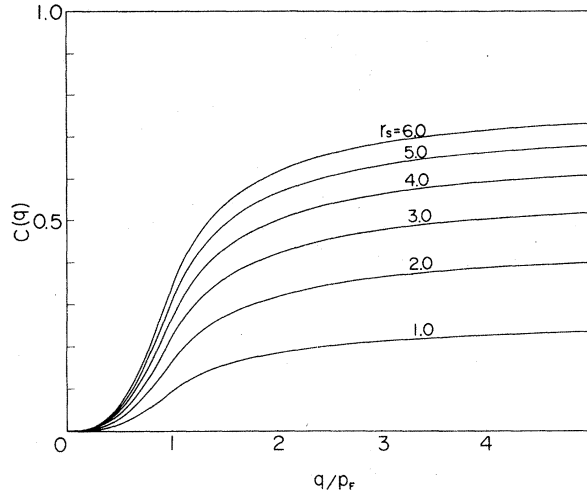


FIG. 3. Calculations of the local field correction  $C(q)$  arising from only spin-antiparallel correlation for various values of  $r_s$ .

### B. $\Gamma(p)$

The energy width  $\Gamma(p)$  has been numerically calculated for various electron densities using values of  $G(q)$  and  $C(q)$  obtained in the preceding section. Calculated values of  $\Gamma(p)$  by the present theory together with those in the RPA are shown in Fig. 4 for  $r_s = 2.0$ . The energy width is composed of two contributions<sup>17</sup>: One comes from particle-hole pair excitations and the other from virtual-plasmon excitations. In the immediate vicinity of  $p_F$   $\Gamma(p)$  is proportional to  $(p - p_F)^2$ . As  $p$  goes away from  $p_F$  it does not continue to increase in such a manner but becomes rather small, so far as  $p \lesssim p_F + q_c$ . The energy width increases drastically at the threshold wave number near  $p_F + q_c$  where a damping channel due to a plasmon-emitting process opens. Such a qualitative behavior of  $\Gamma(p)$  as a function of  $p$  is common to the two calculations. For the quantitative estimation of  $\Gamma(p)$  in the metallic region, however, it is necessary to take the local field correction into account. The magnitude of  $\Gamma(p)$  evaluated by the present theory is reduced, compared with that in the RPA, for all values of  $p$  except a very small interval around the threshold wave number. When  $p$  is apart from the Fermi wave number, roughly by an amount of  $p_F$ , the reduction caused by the local field correction is pronounced. It is owing chiefly to the reduction of the contribution from the particle-hole pair excitations. On the other hand, the contribution from plasmon excitations is rather

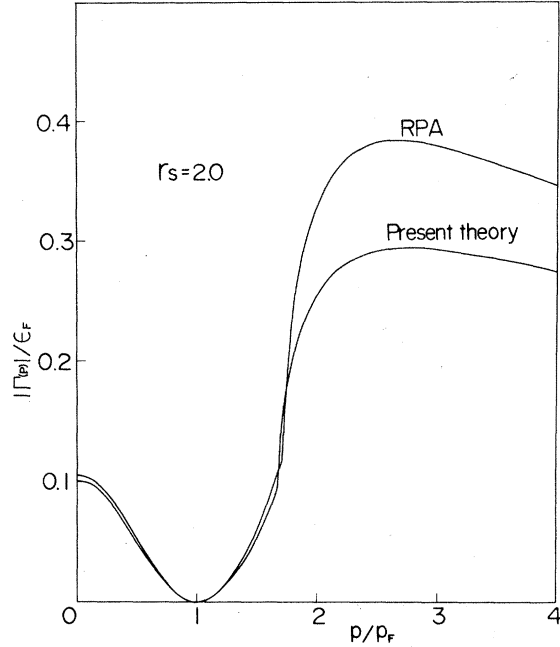


FIG. 4. Calculations of the energy width  $\Gamma(p)$  in the present theory and the RPA for  $r_s = 2.0$ .

insensitive to the local field correction, since the coupling between a plasmon and an electron is associated with small momentum transfers.

The ratio of  $\Gamma(p)$  to the quasiparticle energy measured from the Fermi level takes its maximum value

$$|\Gamma(p)| / (\epsilon_p - \epsilon_F) \simeq 0.1,$$

at a certain wave number somewhat larger than  $p_F + q_c$ . The magnitude of  $\Gamma(p)$  itself attains its maximum value,  $0.295\epsilon_F$  at  $p = 2.8p_F$ , where the ratio of  $\Gamma(p)$  to the quasiparticle energy is smaller (0.04). This fact supports that the quasiparticle picture is still available even for the problem related to the intermediate excitations.

The cutoff wave number  $q_c$  is usually defined as a position at which the plasmon joins the one-pair excitation region. The value of  $q_c$  calculated with the dielectric function defined by Eq. (8) is  $0.68p_F$  for  $r_s = 2.0$ , while the RPA one is  $0.73p_F$ . The threshold wave number is reduced roughly by the same amount.

The variation of  $\Gamma(p)$  with respect to the electron density can be seen in Fig. 5. As  $r_s$  becomes larger, the magnitude of  $\Gamma(p)$  increases generally except for a small interval around the threshold wave number. It should be noted here that the reduction of  $\Gamma(p)$  caused by the local field correc-

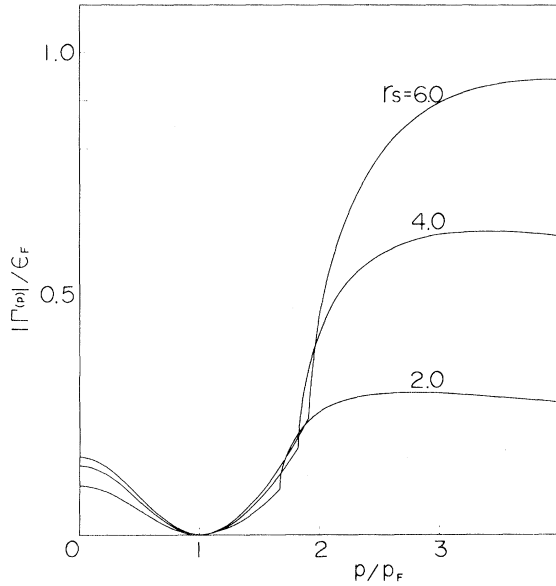


FIG. 5. Calculations of the energy width  $\Gamma(p)$  in the present theory for  $r_s=2.0, 4.0,$  and  $6.0$ .

tion is much more pronounced for  $r_s=4.0, 6.0$  than the case of  $r_s=2.0$ ; the curve of  $\Gamma(p)$  calculated in the RPA for  $r_s=4.0$  amounts roughly to the one by the present theory for  $r_s=6.0$  shown in Fig. 5. The maximum of  $\Gamma(p)$  increases roughly in proportion to  $r_s$ . The ratio of  $\Gamma(p)$  to the quasiparticle energy measured from the Fermi level at the maximum point increases as  $r_s$  becomes larger. The threshold wave number by the present theory increases more gently than that in the RPA as  $r_s$  increases.

### III. DISPERSION AND DAMPING OF PLASMON

The plasmon is a well-defined excitation for  $q \leq q_c$ . Its dispersion can be written as  $\omega_{pl}(q) = \omega_{pl} + \xi q^2 + \dots$  for very small  $q$ . The exact expression for the coefficient  $\xi$  is obtained from the third frequency moment. Perturbation calculations of a damping of the plasmon have been performed<sup>18-20</sup> since the first attempt by DuBois.<sup>10</sup> These calculations are valid only for small wave number  $q \ll q_c$ . The dispersion and damping of the plasmon at metallic densities, however, have not yet been understood in a satisfactory manner except such an extremely long-wavelength region. We shall study here the dispersion and damping of the plasmon, giving particular attention to their behaviors in the vicinity of  $q_c$ . In the

preceding section we have estimated  $q_c$  from the dielectric function of Eq. (8) which includes the local field correction alone. Inclusion of the quasiparticle's damping in the expression for the dielectric function furthermore reduces the value of  $q_c$ .

The pole of the inverse dielectric function is related to the plasmon excitation. The imaginary part of the inverse dielectric function is written as

$$\text{Im} \left[ \frac{-1}{\epsilon(q, \omega)} \right] = \frac{\epsilon_2(q, \omega)}{\epsilon_1(q, \omega)^2 + \epsilon_2(q, \omega)^2}, \quad (11)$$

where  $\epsilon_1(q, \omega)$  and  $\epsilon_2(q, \omega)$  denote the real and imaginary parts of the dielectric function, respectively. In the RPA the dispersion curve of the plasmon determined by the equation  $\epsilon_1(q, \omega) = 0$  is quite equivalent to the peak in  $S(q, \omega)$ , since higher-order corrections giving the damping of the plasmon are not allowed for there. In the quasi-one-pair excitation approximation, Eq. (11) can be reduced into a scaled form:

$$\text{Im} \left[ \frac{-1}{\epsilon(q, \omega)} \right] = \frac{1}{1 - G(q)} \frac{\tilde{\epsilon}_2(q, \omega)}{\tilde{\epsilon}_1(q, \omega)^2 + \tilde{\epsilon}_2(q, \omega)^2}. \quad (12)$$

Here,  $\tilde{\epsilon}_1(q, \omega)$  and  $\tilde{\epsilon}_2(q, \omega)$  are given as follows:

$$\tilde{\epsilon}_1(q, \omega) = 1 + [1 - G(q)]v(q)\tilde{\pi}_1^0(q, \omega), \quad (13)$$

$$\tilde{\epsilon}_2(q, \omega) = [1 - G(q)]v(q)\tilde{\pi}_2^0(q, \omega), \quad (14)$$

where  $\tilde{\pi}_1^0(q, \omega)$  and  $\tilde{\pi}_2^0(q, \omega)$  denote the real and imaginary parts of  $\tilde{\pi}^0(q, \omega)$  defined by Eq. (4), respectively. Let us consider Eq. (12). For the understanding of the spectral shape of  $S(q, \omega)$  for  $q$  smaller than  $p_F$  it is advisable to investigate solutions of  $\tilde{\epsilon}_1(q, \omega) = 0$  instead of  $\epsilon_1(q, \omega) = 0$ , although the solution of  $\tilde{\epsilon}_1(q, \omega) = 0$  is different in a subtle way from that of  $\epsilon_1(q, \omega) = 0$ . The precise behavior of the solutions dominates the spectral shape of  $S(q, \omega)$  in the vicinity of  $q_c$ . Solutions of  $\tilde{\epsilon}_1(q, \omega) = 0$  indicate, with reasonable accuracy, the position of the plasmon peak and that of the individual excitation peak immersed in the continuum.

In Fig. 6 the solution of  $\tilde{\epsilon}_1(q, \omega; [G, \Gamma]) = 0$  (case III) as well as that of  $\epsilon_1^{\text{RPA}}(q, \omega) = 0$  (case I) is plotted as a function of  $q$  for  $r_s = 4.0$ . In order to illustrate the importance of the energy width  $\Gamma(p)$  in the vicinity of  $q_c$ , we also plot there the solution of  $\tilde{\epsilon}_1(q, \omega; [G, \Gamma = 0]) = 0$  (case II), where only the

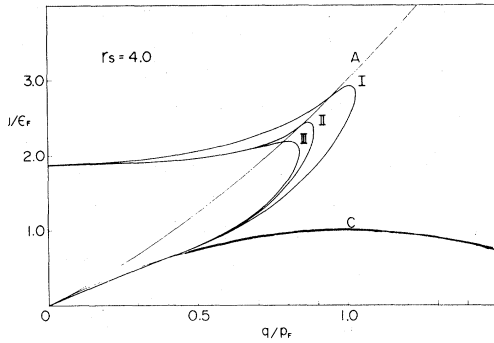


FIG. 6. Solutions of  $\epsilon_1^{\text{RPA}}(q, \omega)$  (I),  $\tilde{\epsilon}_1(q, \omega; [G, \Gamma=0])=0$  (II), and  $\tilde{\epsilon}_1(q, \omega; [G, \Gamma])=0$  (III) for  $r_s=4.0$  are plotted as a function of  $q/p_F$ . Line A indicates the upper bound of one-pair excitation  $\omega/\epsilon_F=(q/p_F)^2+2q/p_F$ . Line C indicates the characteristic boundary  $\omega/\epsilon_F=2q/p_F-(q/p_F)^2$ .

local field correction is taken into account. Each of these three equations has two solutions for a value of  $q$  smaller than a certain wave number somewhat larger than  $q_c$ . The upper solutions correspond to the plasmon mode; these solutions in cases I and II where the energy width is not included are situated precisely at plasmon peaks in their  $S(q, \omega)$ . As  $q$  approaches  $q_c$ , the upper curve in case I becomes still steeper and is tangent to the upper bound of one-pair excitations at  $q=q_c$  where the relation  $\omega_{pl}(q)=\epsilon_{p_F+q}-\epsilon_F$  holds. The curve in case II is located inside the RPA curve. The plasmon dispersion in case II is lowered, compared with that in the RPA; as  $q$  approaches  $q_c$ , it increases in such a way that it is also tangent to the upper bound at  $q=q_c$ . The value of  $q_c$  in case II is reduced by a considerable amount. The curve in case III is located inside those in cases I and II. The plasmon dispersion in case III is not shifted appreciably from that in case II for  $q \lesssim 0.7p_F$  but it is significantly lowered as  $q$  approaches an intersecting point of the plasmon curve and the upper bound, compared with case II. It is noted here that the two curves in case III are not tangent but are intersecting. The lowering of the plasmon dispersion in case III around the intersecting point originates from the drastic increase of  $\Gamma(p)$  arising from plasmon emission. The plasmon peak in  $S(q, \omega)$  in case III is shifted somewhat to the low-energy side from the solution of  $\tilde{\epsilon}_1(q, \omega; [G, \Gamma])=0$  since  $\tilde{\epsilon}_2(q, \omega; [G, \Gamma])$  does not vanish there. Strictly speaking, the conventional definition of  $q_c$  is not available when  $\Gamma(p)$  is included. Instead, we shall name here the above intersecting point as a cutoff wave number. Similar curves in the cases of I—III

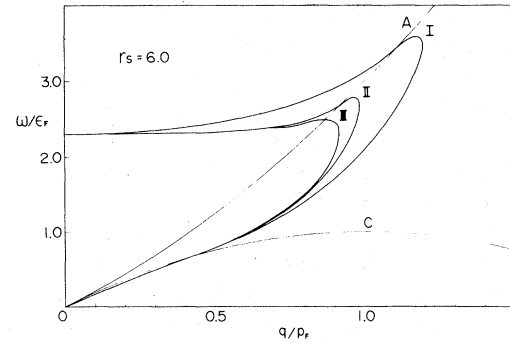


FIG. 7. Solutions of  $\epsilon_1^{\text{RPA}}(q, \omega)=0$  (I),  $\tilde{\epsilon}_1(q, \omega; [G, \Gamma=0])=0$  (II), and  $\tilde{\epsilon}_1(q, \omega; [G, \Gamma])=0$  (III) for  $r_s=6.0$  are plotted as a function of  $q/p_F$ . Lines A and C have the same meaning as in Fig. 6.

are also plotted for  $r_s=6.0$  in Fig. 7 where one can see that the above situation around  $q_c$  is more pronounced. Thus, the plasmon dispersion in the vicinity of  $q_c$  is strongly affected by the local field correction  $G(q)$  and the energy width  $\Gamma(p)$ . In Fig. 8 values of  $q_c$  estimated in the above three approximations are plotted as a function of  $r_s$ . As the electron density is lowered, the value of  $q_c$  calculated in the RPA increases monotonously and exceeds the Fermi wave number  $p_F$  about at  $r_s=5.0$ . Such a behavior of  $q_c$  as a function of the electron density is not reasonable, since the wavelength of the collective oscillation should be,

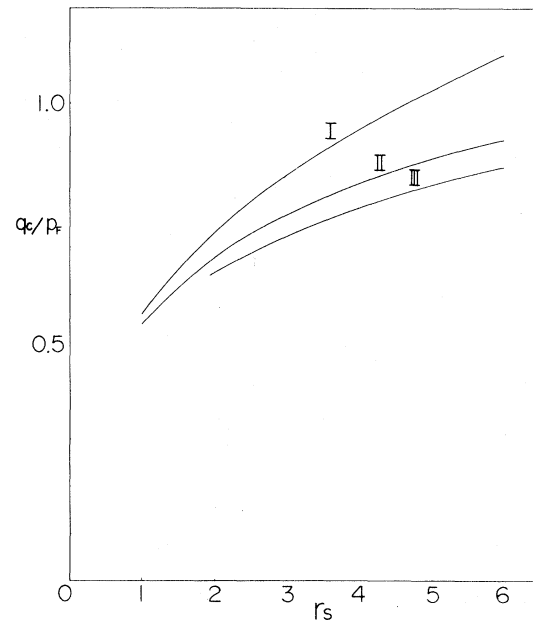


FIG. 8. Values of  $q_c$  estimated from  $\epsilon_1^{\text{RPA}}(q, \omega)$  (I),  $\tilde{\epsilon}_1(q, \omega; [G, \Gamma=0])$  (II), and  $\tilde{\epsilon}_1(q, \omega; [G, \Gamma])$  (III) are plotted as a function of  $r_s$ .

at least, of the order of interparticle distance. Experimentally observed values<sup>3-7</sup> of  $q_c$  for real metals appear to be still smaller than that predicted from the RPA. Even at the highest metallic density the value of  $q_c$  evaluated in the quasi-one-pair excitation approximation is reduced by an appreciable amount, compared with the RPA result. The reduction of  $q_c$  is much more pronounced as the electron density is lowered.

Finally, spectral shapes of  $S(q, \omega)$  for some typical values of  $q$  smaller than  $p_F$  are shown for  $r_s = 2.0$  in Fig. 9. Even for  $q$  much smaller than  $q_c$  the plasmon has a finite width. Such a damping of the plasmon is caused by implicit inclusion of two-pair excitations in the framework of the quasi-one-pair excitation approximation. According to standard perturbation calculations of a damping of the plasmon, the contribution from two-pair excitations is of order  $q^2$  for small  $q$ , while that from one-pair-one-plasmon excitations is much smaller and is of order  $q^6$ .<sup>19</sup> But when  $q$  approaches the vicinity of  $q_c$  a straightforward per-

turbation calculation is of no use, as has been explained in Sec. IV of the preceding paper. In a wave-number region that is neighboring the one-pair continuum, a coupling between one-pair excitations and one-pair-one-plasmon or two-pair excitations must be allowed for, which is successfully achieved in the quasi-one-pair excitation approximation. The quasiparticle state starts to decay drastically when its wave number exceeds a certain value about  $p_F + q_c$ , as has been mentioned in Sec. II. Correspondingly, the width of the plasmon peak increases abruptly in the immediate vicinity of  $q_c$ .

#### IV. DOUBLE-PEAK STRUCTURE IN THE INTERMEDIATE WAVE-NUMBER REGION

In this section we give a theoretical interpretation of the double-peak structure observed first at Bell Laboratories<sup>7</sup> using inelastic x-ray scattering. An anomalous behavior of the plasmon dispersion around  $q_c$  observed in electron scattering experiments<sup>3-6</sup> is also interpreted. The peak position of the spectra of  $S(q, \omega)$  for  $q \lesssim q_c$  is almost dominated by the solution of  $\tilde{\epsilon}_1(q, \omega) = 0$ , as has been explained in Sec. III. The equation  $\tilde{\epsilon}_1(q, \omega) = 0$ , however, has no solution for  $q$  larger than about  $q_c$ . As  $q$  increases from  $q_c$ , the local field correction and the energy width of the quasiparticle play a much more important role. The frequency dependence of  $\tilde{\epsilon}_1(q, \omega)$  becomes much gentler. The spectral shape of  $\tilde{\epsilon}_2(q, \omega)$ , on the other hand, starts to be modified in a remarkable manner. Consequently, the spectral shape of  $S(q, \omega)$  in the intermediate wave-number region depends chiefly on the spectral structure in  $\tilde{\epsilon}_2(q, \omega)$ ; the denominator in Eq. (12) has a minor effect. Numerical calculations of  $S(q, \omega)$  have been performed for various electron densities,  $r_s = 1.5, 2.0, 3.0, 4.0,$  and  $6.0$ .

##### A. Spectral structure for $r_s = 2.0$

We first discuss the numerical result for  $r_s = 2.0$  in comparison with the experimental spectra<sup>7</sup> for Be ( $r_s = 1.88$ ), since the double-peak structure for Be was observed distinctly by Platzman and Eisenberger. Calculated spectra of  $S(q, \omega)$  for  $r_s = 2.0$  are shown in Fig. 10 for various wave numbers. Experimental spectra for Be are shown in Fig. 11. A plasmonlike peak accompanied with a well-developed shoulder or a broad peak can be

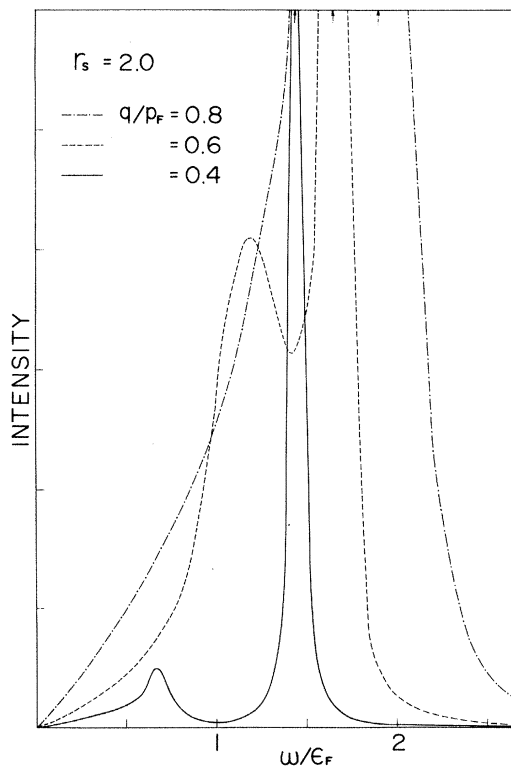


FIG. 9. Calculated intensities of  $S(q, \omega)$  in the present theory for  $r_s = 2.0$  are shown as a function of  $\omega/\epsilon_F$  for  $q/p_F = 0.4, 0.6,$  and  $0.8$ . The peak position of  $S(q, \omega)$  for each case is indicated by the corresponding upward arrow.

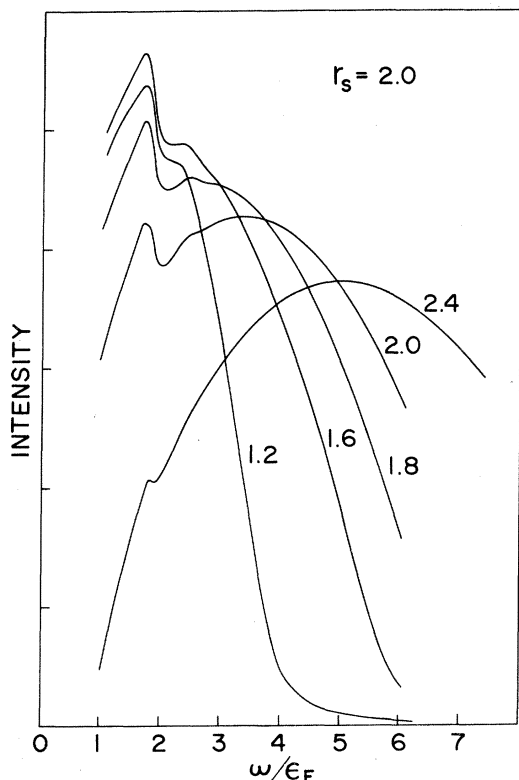


FIG. 10. Calculated intensities of  $S(q, \omega)$  in the present theory for  $r_s = 2.0$  are shown as a function of  $\omega/\epsilon_F$  for  $q/p_F = 1.2, 1.6, 1.8, 2.0,$  and  $2.4$ . The intensity is measured on the same scale as in Fig. 9.

reproduced very well by the present calculation. As  $q$  increases, the calculated spectral shape of  $S(q, \omega)$  varies in a quite similar manner as the observed one. Let us follow the variation of the spectral shape from the wave number where the crossing over of the plasmonlike peak and the individual excitation peak occurs, up to the wave numbers beyond  $2p_F$ . About at  $q = 0.8p_F$  the plasmon and individual excitation peaks make up a unified peak with very high intensity, which is located at  $1.9\epsilon_F$  (see Fig. 9). For  $0.9p_F < q < 1.5p_F$  a considerably sharp plasmonlike peak still appears and is accompanied with a shoulder on the high-energy side. It is noted that the intensity of the plasmonlike peak is much smaller than that of the maximum plasmon peak at  $q = 0.8p_F$ ; intensities of  $S(q, \omega)$  in Figs. 9 and 10 are measured on the same scale. The existence of the plasmonlike peak of  $S(q, \omega)$  can be traced back to the sudden increase on  $\Gamma(p)$ . But its position is still affected by the frequency dependence of  $\tilde{\epsilon}_1(q, \omega)$ ; even for  $q$  somewhat larger than  $0.8p_F$   $\tilde{\epsilon}_1(q, \omega)$  takes a value

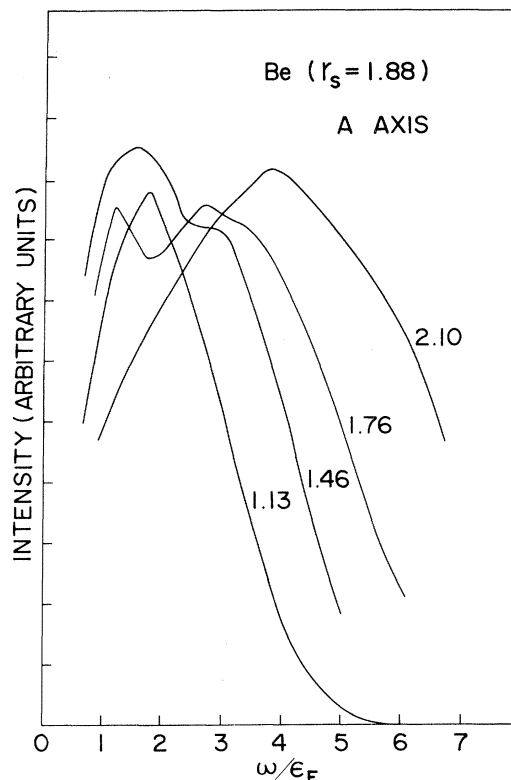


FIG. 11. Observed intensities of  $S(q, \omega)$  for Be along the A axis in x-ray scattering experiments (Ref. 7) are shown as a function of  $\omega/\epsilon_F$  for  $q/p_F = 1.13, 1.40, 1.76,$  and  $2.10$ .

much smaller than 1 about at the maximum frequency of the plasmon,  $1.9\epsilon_F$ . For  $1.5p_F < q < 2.0p_F$  the well-developed shoulder grows into a broad peak. It corresponds to the usual individual excitation peak. For  $q > 1.5p_F$  the spectral shape of  $S(q, \omega)$ , as a whole, is almost equivalent to that of  $\tilde{\epsilon}_2(q, \omega)$ . The effects of  $\tilde{\epsilon}_1(q, \omega)$  are of little importance there. The position of the plasmonlike peak of  $S(q, \omega)$  is located about at  $1.7\epsilon_F$  and is shifted to the high-energy side by only an amount smaller than  $0.1\epsilon_F$ , compared with the corresponding peak of  $\tilde{\epsilon}_2(q, \omega)$ .

The experimental<sup>7</sup>  $S(q, \omega)$  for Al corresponding to  $r_s = 2.0$  has been reported only for  $q = 1.6p_F$ , which consists of a plasmonlike peak and a well-developed shoulder. The calculated spectrum for  $q = 1.6p_F$  shows an appreciable splitting into the two peaks. Considering resolving power, one may say that it is in very good agreement with the experimental result.

As  $q$  increases, the strength of the broad peak develops relative to that of the sharper one. About

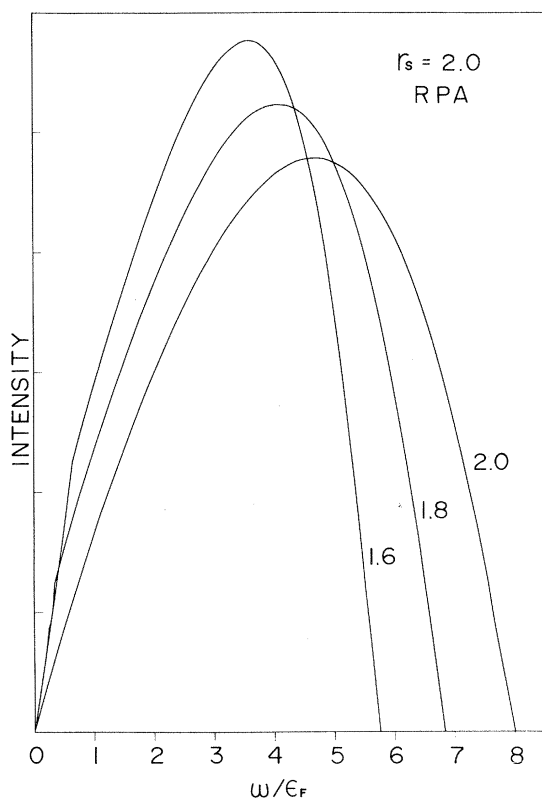


FIG. 12. Calculated intensities of  $S(q, \omega)$  in the RPA for  $r_s = 2.0$  are shown as a function of  $\omega/\epsilon_F$  for  $q/p_F = 1.6, 1.8,$  and  $2.0$ .

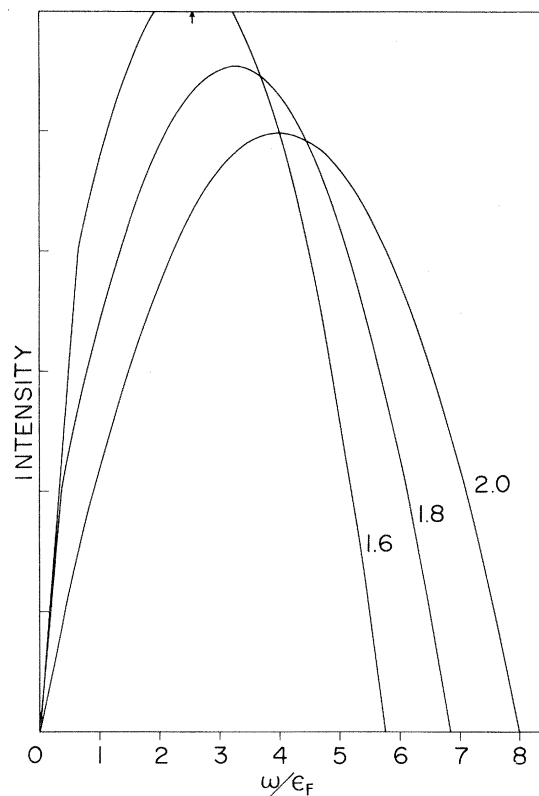


FIG. 13. Calculated intensities of  $S(q, \omega)$  for the noninteracting system are shown as a function of  $\omega/\epsilon_F$  for  $q/p_F = 1.6, 1.8,$  and  $1.0$ .

at  $q = 2.0p_F$ , a switching over of the two strengths occurs. For  $q > 2.0p_F$  the strength of the sharper peak becomes weaker and fades away as  $q$  increases. But even at  $q = 2.5p_F$ , a weak shoulder as the continuation of the plasmonlike peak can be discerned.

Much attention has been paid to the negative dispersion<sup>7</sup> of the plasmonlike peak observed in the intermediate wave-number region. The present calculation shows negative dispersion for  $0.8p_F < q < 1.4p_F$  (see Fig. 14 below). For  $q < 0.8p_F$  the spectral shape of  $S(q, \omega)$  is almost dominated by the solutions of  $\tilde{\epsilon}_1(q, \omega) = 0$ . For  $q > 1.5p_F$ , on the other hand, the spectral shape is almost ascribed to  $\tilde{\epsilon}_2(q, \omega)$ . The negative dispersion manifests itself in the transitional region.

On the high-energy side of the one-pair excitation region there appears a tail, which is in agreement with the experimental observation. The calculated spectra in the intermediate wave-number region, as a whole, are shifted to the low-energy side, compared with those in the RPA. Specifically the position of the broad peak for  $q = 1.6p_F$  is

shifted by an amount of  $1.3\epsilon_F$ . For comparison calculated spectra of  $S(q, \omega)$  in the RPA and those for the noninteracting system are shown for several wave numbers in Figs. 12 and 13, respectively. If one takes only the local field correction, there appears no fine structure in  $S(q, \omega)$ . The peak position in such a case is lowered but it is situated at a frequency higher than that of the noninteracting system. The energy width gives rise to the fine structure consisting of the sharp plasmonlike peak and the broad peak. It shifts, furthermore, the position of the broad peak to a frequency lower than that of the noninteracting system. Apart from the fine structure and the tail, the calculated spectrum in the present theory, as a whole, bears a closer resemblance to that of the noninteracting system rather than to that in the RPA. One may then say that  $S(q, \omega)$  of the noninteracting system is the better for a starting approximation in the intermediate wave-number region.

The distinct double-peak or the one-peak—one-shoulder structure in the present calculation could not possibly be destroyed, even if convoluted with

an experimental resolution function of width 5 eV; the width of 5 eV is less than half of the measuring unit used in Fig. 10. We shall note here that in our calculated spectra the broad peak is accompanied with a small dip located about at  $3.0\epsilon_F$ . Such a small dip is certainly flattened in the experiments carried out at Bell Laboratories but it could be observed if much higher resolving power is at-

tained. It may be worthwhile to clarify here the origin of the plasmonlike peak and the broad peak together with that of the small dip. Let us denote by  $p_c$  the threshold wave number where the damping channel due to virtual plasmon excitations opens (see Fig. 4). Then,  $\tilde{\pi}_2^{(0)}(q, \omega)$  can formally be separated into three parts as follows:

$$\begin{aligned} \tilde{\pi}_2^{(0)}(q, \omega) = & 2 \int_{|\vec{p} + \vec{q}| < p_c} \frac{d\vec{p}}{(2\pi)^3} f(p)[1 - f(\vec{p} + \vec{q})] \frac{\Gamma(p) - \Gamma(\vec{p} + \vec{q})}{(\omega + \epsilon_p - \epsilon_{\vec{p} + \vec{q}})^2 + [\Gamma(p) - \Gamma(\vec{p} + \vec{q})]^2} \\ & + 2 \int_{|\vec{p} + \vec{q}| > p_c} \frac{dp}{(2\pi)^3} f(p)[1 - f(\vec{p} + \vec{q})] \frac{\Gamma(p) - \Gamma(\vec{p} + \vec{q})}{(\omega + \epsilon_p - \epsilon_{\vec{p} + \vec{q}})^2 + [\Gamma(p) - \Gamma(\vec{p} + \vec{q})]^2} \\ & - 2 \int \frac{dp}{(2\pi)^3} f(\vec{p} + \vec{q})[1 - f(p)] \frac{\Gamma(\vec{p} + \vec{q}) - \Gamma(p)}{(\omega + \epsilon_p - \epsilon_{\vec{p} + \vec{q}})^2 + [\Gamma(p) - \Gamma(\vec{p} + \vec{q})]^2}. \end{aligned} \quad (15)$$

The first term on the right-hand side of Eq. (15) includes a rather small energy width, since  $|\vec{p} + \vec{q}| < p_c$ . Its spectral shape is very similar to that for the noninteracting system when  $\omega \lesssim \omega_{pl}$ . For  $\omega \gtrsim \omega_{pl}$ , however, the spectrum decreases abruptly, forming a cusp about at  $\omega_{pl}$ , and almost vanishes at  $\omega = \epsilon_{p_c} - \epsilon_{p_c} - q$ . The small dip can be

traced back to this terminating frequency of the spectrum of the first term. On the other hand, the second term makes a contribution to the broad peak. The third term is of little importance for  $\omega > 0$ .

In Fig. 14 the calculated dispersion curve of the plasmon and the plasmonlike peak as well as that

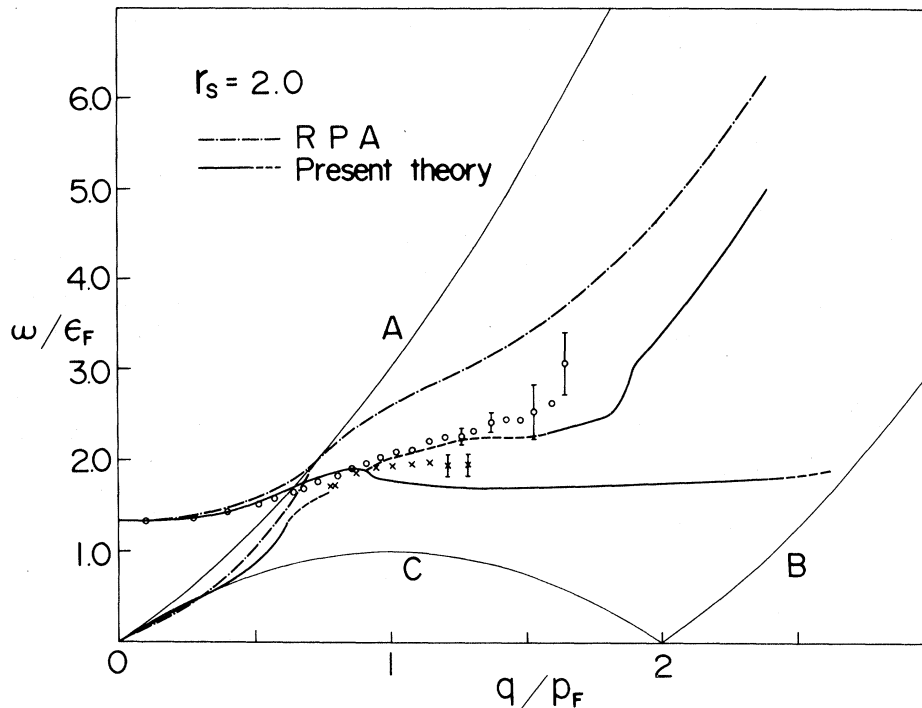


FIG. 14. Calculated positions of the plasmon peak and its continuation together with those of the individual excitation peak are shown as a function of  $q/p_F$ . The open circles denote the experimental results by Batson *et al.* (Ref. 5) and the crosses those by Zacharias (Ref. 4). Lines A and C have the same meaning as in Fig. 6. Line B indicates the lower bound of one-pair excitations  $\omega/\epsilon_F = (q/p_F)^2 - 2q/p_F$ .

of the individual excitation peak is shown in comparison with the observed ones in electron scattering experiments.<sup>4,5</sup> The corresponding dispersion curve in the RPA is also drawn there. The position of the plasmon peak starts from the plasma frequency  $1.33\epsilon_F$  at  $q=0$ . Just before  $q_c$  our dispersion curve bends appreciably from the RPA one. Its continuation into the one-pair continuum exhibits a very small dispersion, compared with the RPA result. Excellent agreement with the experimental observation has thus been obtained. The fine structure for  $q > 0.9p_F$  has not yet been observed in the electron scattering experiments. But even for  $q > 0.9p_F$  the observed dispersion curve by electron scattering is in very good agreement with the calculated location of the well-developed shoulder. It might be reasonably interpreted, if one averages the calculated fine structure over appropriate width of frequency.

#### B. Spectral structure for other densities

We shall examine how the spectral shape of  $S(q, \omega)$  varies with the electron density. The spectral shape of  $S(q, \omega)$  for  $r_s = 1.5$  which corresponds roughly to an averaged density of graphite ( $r_s = 1.53$ ) has been calculated. The fine structure can also be obtained in the intermediate wave-number region. The plasmonlike peak and the well-developed shoulder or the broad peak are very similar to those for  $r_s = 2.0$ . The plasmonlike peak for  $r_s = 1.5$  is somewhat sharper and its intensity is stronger, compared with the case for  $r_s = 2.0$ . The well-developed shoulder grows into the broad peak at a wave number somewhat smaller than that for  $r_s = 2.0$ . A switching over of the two strengths occurs at  $q = 1.9p_F$ .

We shall next mention the spectral shape for  $r_s$  larger than 2.0. The calculated spectra for  $r_s = 3.0$  appropriate roughly for Li ( $r_s = 3.22$ ) and 4.0 are shown for several wave numbers in Figs. 15 and 16, respectively. Note that the fine structure becomes less pronounced as the electron density is lowered. The width of the plasmonlike peak becomes much broader and its intensity is weaker, compared with the case for  $r_s = 2.0$ . The position of the plasmon and the plasmonlike peak measured in units of  $\epsilon_F$  is shifted to the high-energy side. The location of the well-developed shoulder and the broad peak measured in units of  $\epsilon_F$  is, by a small amount, shifted to the low-energy side. As the electron density is lowered, it is more difficult

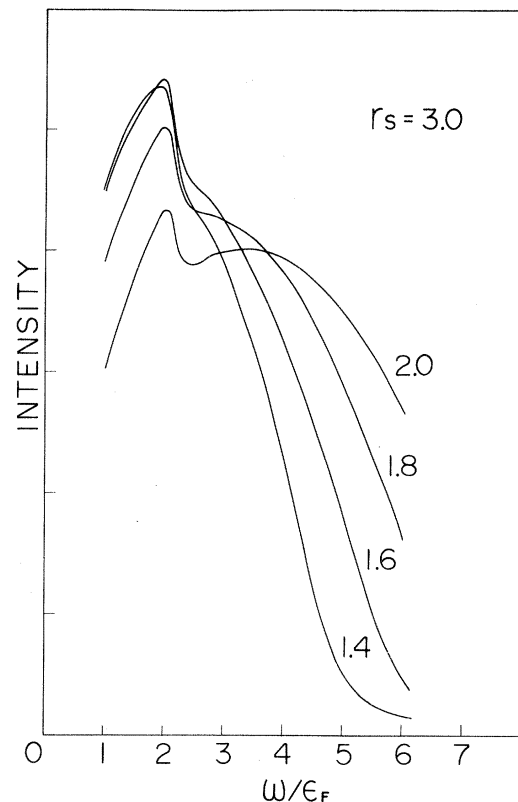


FIG. 15. Calculated intensities of  $S(q, \omega)$  in the present theory for  $r_s = 3.0$  are shown as a function of  $\omega/\epsilon_F$  for  $q/p_F = 1.4, 1.6, 1.8,$  and  $2.0$ .

to discern a shoulder from a plasmonlike peak. Even for  $q$  as large as  $1.6p_F$  the two peaks for  $r_s = 4.0$  are still so much overlapped that we can see a unified peak. Then, the shoulder grows into a broad peak at a larger wave number for large value of  $r_s$ ; e.g., for  $r_s = 4.0$  the splitting into the two peaks can somehow be seen for  $q$  as large as  $2p_F$ . A switching over of the two strengths occurs at  $q = 2.2p_F$  for  $r_s = 4.0$ . The above tendency is due to the fact that the local field correction as well as the energy width plays a more important role as the electron density is lowered. The intensity of the broad peak as well as that of the plasmonlike peak is weakened by a considerable amount, according as the high-energy tail grows. The whole spectral shape becomes much blunter owing to effects of the energy width  $\Gamma(p)$ .

For comparison experimental spectra for Li by Platzman, Eisenberger, and Schmidt<sup>7</sup> are shown in Fig. 17. A shoulder can be discerned for  $q$  as large as  $1.4p_F$ , whose spectral shape has a resemblance to the calculated one for  $r_s = 3.0$ . The shoulder ob-

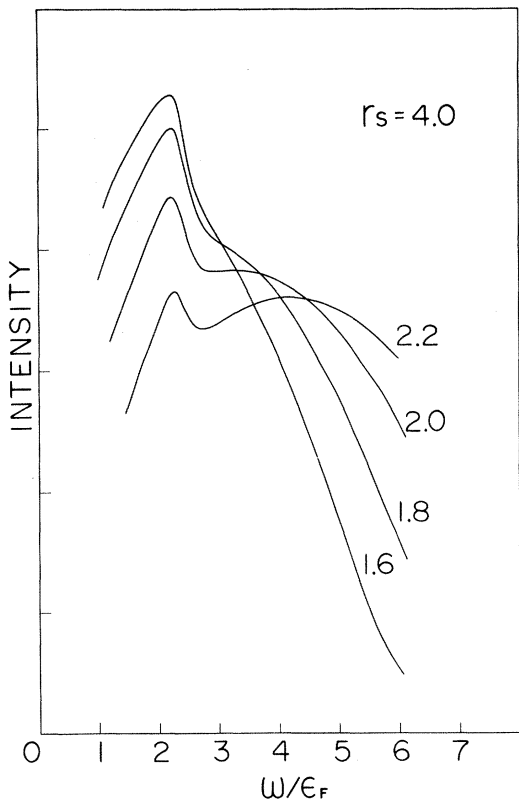


FIG. 16. Calculated intensities of  $S(q,\omega)$  in the present theory for  $r_s=4.0$  are shown as a function of  $\omega/\epsilon_F$  for  $q/p_F=1.6, 1.8, 2.0,$  and  $2.2$ .

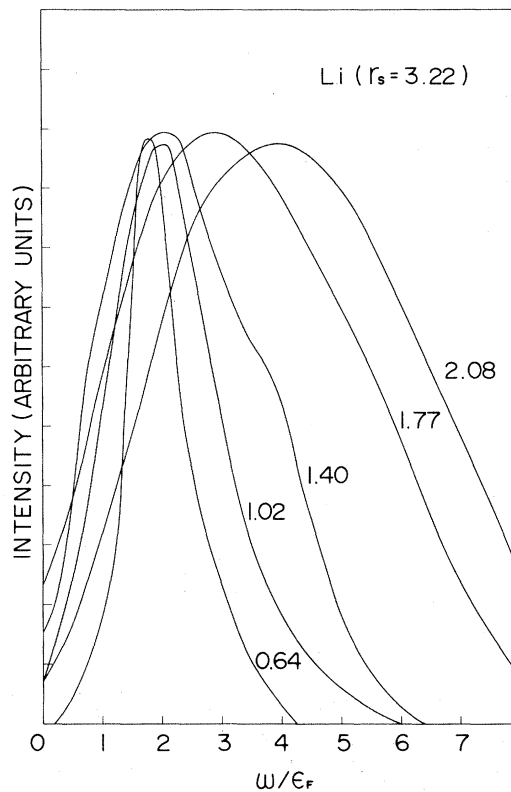


FIG. 17. Observed intensities of  $S(q,\omega)$  for Li in x-ray scattering experiments (Ref. 7) are shown as a function of  $\omega/\epsilon_F$  for  $q/p_F=0.64, 1.02, 1.40, 1.77,$  and  $2.08$ .

served at about  $q=1.4p_F$  is still smaller than the corresponding one for Be ( $r_s=1.88$ ). Priftis, Boviatis, and Vradis<sup>8</sup> have also performed x-ray scattering experiments for Li from  $q=1.8p_F$  to  $q$  as large as  $3p_F$  (see Figs. 18–20). The observed spectra exhibit the plasmonlike peak and the broad peak in a distinct manner. Their experimental spectral shapes are in good agreement with our theoretical results for  $r_s=3.0$ . A separation of their spectrum into two peaks occurs about at  $q=1.8p_F$  which is larger than the corresponding wave number for Be. Such a variation of the observed spectral shape with the electron density is consistent with the aforementioned theoretical prediction. We note here that the general behavior of dispersion curves of the plasmonlike peak and the broad peak observed by Priftis, Boviatis, and Vradis bears a close resemblance to that of our theoretical dispersion curves shown in Fig. 14.

X-ray scattering experiments for graphite have been performed along two directions by Eisenberger and Platzman.<sup>7</sup> Experimental spectra of

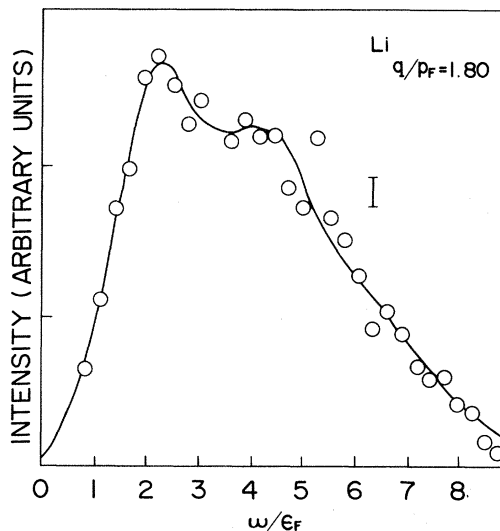


FIG. 18. Observed intensity of  $S(q,\omega)$  for Li in x-ray scattering experiments (Ref. 8) are shown as a function of  $\omega/\epsilon_F$  for  $q/p_F=1.80$ .

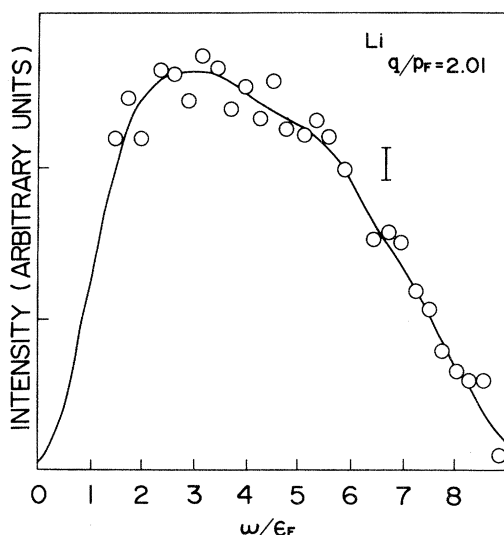


FIG. 19. Observed intensity of  $S(q, \omega)$  for Li in x-ray scattering experiments (Ref. 8) are shown as a function of  $\omega/\epsilon_F$  for  $q/p_F=2.01$ .

graphite are shown for  $q=1.42p_F$  in Fig. 21. The graphite has the layer structure. The result along the A axis parallel to the layer reveals a plasmon-like peak sharper than that for Be and a shoulder. The result along the C axis perpendicular to the layer, however, shows no structure (see Fig. 21). The averaged distance between electrons along the A axis is shorter than that corresponding to the averaged density  $r_s=1.53$ . The averaged distance

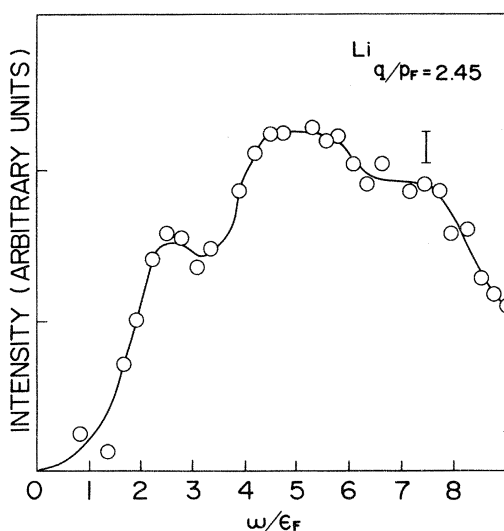


FIG. 20. Observed intensity of  $S(q, \omega)$  for Li in x-ray scattering experiments (Ref. 8) are shown as a function of  $\omega/\epsilon_F$  for  $q/p_F=2.45$ .

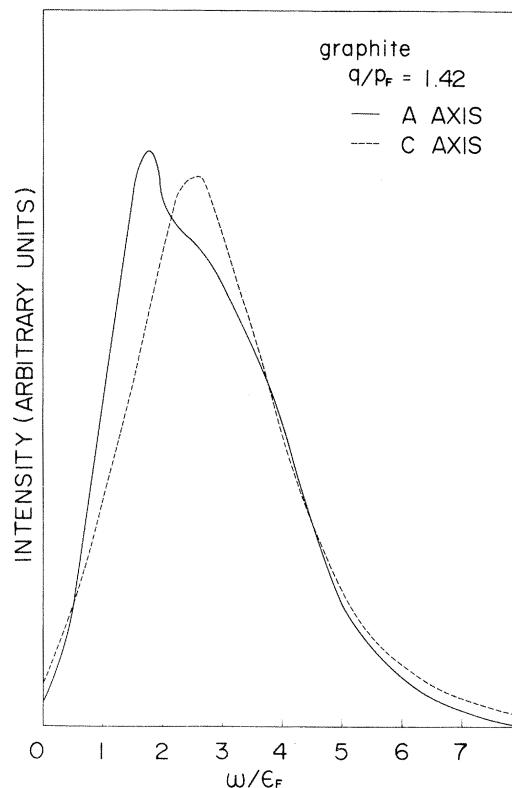


FIG. 21. Observed intensities of  $S(q, \omega)$  for graphite along the A and C axes in x-ray scattering experiments (Ref. 7) are shown as a function of  $\omega/\epsilon_F$  for  $q/p_F=1.42$ .

along the C axis, on the other hand, is longer and is equivalent to a larger value of  $r_s$  ( $r_s=3.5$ ). One may consequently say that even the experimentally observed anisotropy of the spectral shape of graphite is understood qualitatively by the present theory.

## V. CONCLUDING REMARKS

The existence of the plasmonlike peak and the broad peak in the intermediate wave-number region was first observed by Platzman and Eisenberger, and was confirmed by Priftis, Boviatsis, and Vradis. A controversy on its theoretical interpretation has, however, dragged on without much success. After critical examinations of several guiding principles hitherto used and further considerations based on diagrammatic analysis, we have obtained the quasi-one-pair excitation approximation in the preceding paper. In this paper the numerical study on the basis of the quasi-one-pair excitation ap-

proximation has thus succeeded in explaining the observed double-peak structure as well as the unexpected dispersion of the plasmon around  $q_c$ , without any adjustable parameter. Their physical origin can be traced back to the characteristic behaviors of the local field correction and the energy width of the quasiparticle. The fine structure consisting of a plasmonlike peak and a broad peak or a shoulder has commonly been observed for a wide variety of different metals and even for semiconductors such as Si. This may be understood, if one considers that the excitation spectrum as high as the plasmon excitation is little influenced by precise features of low-lying excitation spectra in the vicinity of the Fermi level. So far as the well-defined plasmon excitation is observed for small wave numbers, its continuation into intermediate wave numbers may possibly be observed, since it is ascribed to the striking damping effect of the quasiparticle due to the virtual plasmon excitations under the influence of strong short-range correlations. It is hoped that both x-ray and electron scattering experiments on  $S(q, \omega)$  will be carried out with still higher resolving power.

As a consequence, we may safely say that an electron liquid model with the uniform positive background can be applied for metallic phenomena of intermediate wave numbers as well, so far as one is concerned with intermediate excitations. The notion of a quasiparticle might often be supposed to work well only for phenomena of low-lying excitations. The quasiparticle picture, however, has thus proved to be practically applicable for the problem of intermediate excitations, provided that the energy width of the quasiparticle and the irreducible particle-hole interaction are evaluat-

ed in a quantitative manner at metallic densities. Using their own forms for  $G(q)$  and  $\Gamma(p)$ , Mukhopadhyay, Kalia, and Singwi<sup>21</sup> have first obtained the spectral shape which has some resemblance to the observed one, although the fine structure cannot distinctly be reproduced. Their forms for  $G(q)$  and  $\Gamma(p)$  are not appropriate for the detailed description of the spectral shape. Now we may say that in a sense we have justified their underlying idea from a diagrammatic point of view.

Finally we shall comment on contributions from pure multipair excitations which are beyond the scope of the present calculation. They are incoherent and appear as a broad background. Calculated values of  $S(q, \omega)$  for frequencies much higher than the upper bound of one-pair excitations may be overestimated, although they are extremely small and bear little relation to the spectral structure in  $S(q, \omega)$  in the intermediate excitation region. The asymptotic form of  $S(q, \omega)$  in the quasi-one-pair excitation approximation is of order  $\omega^{-2}$  for high frequencies, while the correct asymptotic form<sup>22</sup> is of order  $\omega^{-11/2}$ . The incoherent contributions of  $S(q, \omega)$  could remedy the overestimation for very high frequencies.

#### ACKNOWLEDGMENTS

We would like to thank Professor H. Takayama and Professor K. Wada for their careful reading of the manuscript. One of the authors (H. Y.) is thankful to Professor M. Suzuki in Tohoku University for informing him of the paper by Priftis, Boviatsis, and Vradis. Numerical calculations were made by Hitac M-200H at Hokkaido University Computing Center.

<sup>1</sup>D. Pines, *Elementary Excitations in Solids* (Benjamin, New York, 1963).

<sup>2</sup>D. Pines and P. Nozieres, *The Theory of Quantum Liquids* (Benjamin, New York, 1966), Vol. I.

<sup>3</sup>D. M. Militosis, *Phys. Rev. B* **3**, 701 (1971).

<sup>4</sup>P. Zacharias, *J. Phys. F* **5**, 645 (1975).

<sup>5</sup>P. E. Batson, C. H. Chen, and J. Silcox, *Phys. Rev. Lett.* **37**, 937 (1976).

<sup>6</sup>P. C. Gibbons, S. E. Schnatterly, J. J. Ritsko, and J. R. Fields, *Phys. Rev. B* **13**, 2451 (1976).

<sup>7</sup>P. Eisenberger, P. M. Platzman, and K. C. Pandey, *Phys. Rev. Lett.* **31**, 311 (1973); P. M. Platzman and P. Eisenberger, *ibid.* **33**, 152 (1974); P. M. Platzman, P. Eisenberger, and P. Schmidt, *ibid.* **34**, 18 (1975); P. Eisenberger and P. M. Platzman, *Phys. Rev. B* **13**,

934 (1976).

<sup>8</sup>G. D. Priftis, J. Boviatsis, and A. Vradis, *Phys. Lett.* **68A**, 482 (1978).

<sup>9</sup>K. Awa, H. Yasuhara, and T. Asahi, preceding paper, *Phys. Rev. B* **25**, 3670 (1982).

<sup>10</sup>D. F. DuBois, *Ann. Phys.* **7**, 174 (1959); **8**, 24 (1959).

<sup>11</sup>J. Hubbard, *Proc. R. Soc. London Ser. A* **240**, 539 (1957); **243**, 336 (1957).

<sup>12</sup>H. Yasuhara, *Solid State Commun.* **11**, 1481 (1972); *J. Phys. Soc. Jpn.* **36**, 361 (1974); *Physica* **78**, 420 (1974).

<sup>13</sup>P. Vashishta and K. S. Singwi, *Phys. Rev. B* **6**, 875 (1972).

<sup>14</sup>D. N. Lowy and G. E. Brown, *Phys. Rev. B* **12**, 2138 (1975); K. Bedell and G. E. Brown, *ibid.* **17**, 4512

- (1978).
- <sup>15</sup>A. A. Kugler, *J. Stat. Phys.* **12**, 35 (1975).
- <sup>16</sup>F. Toigo and T. O. Woodruff, *Phys. Rev. B* **2**, 3958 (1970); **4**, 371 (1971); **4**, 4312 (1971).
- <sup>17</sup>L. Hedin and S. Lundqvist, in *Solid State Physics*, edited by F. Seitz, D. Turnbull, and H. Ehrenreich (Academic, New York, 1969), Vol. 23, p. 1.
- <sup>18</sup>B. W. Ninham, C. J. Powell, and N. Swanson, *Phys. Rev.* **145**, 209 (1966).
- <sup>19</sup>M. Hasegawa and M. Watabe, *J. Phys. Soc. Jpn.* **27**, 1393 (1969).
- <sup>20</sup>D. F. DuBois and M. G. Kivelson, *Phys. Rev.* **186**, 409 (1969).
- <sup>21</sup>G. Mukhopadhyay, R. K. Kalia, and K. S. Singwi, *Phys. Rev. Lett.* **34**, 950 (1975).
- <sup>22</sup>A. J. Glick and W. F. Long, *Phys. Rev. B* **4**, 3455 (1971).